Drizzle in stratocumulus clouds: observations and comparison with models of differing complexity.

ROBERT WOOD[1]

Meteorological Research Flight, Farnborough, UK.

Abstract

Detailed observations of stratocumulus clouds on four days are examined with specific reference to drizzle formation processes. The clouds differed considerably in thickness, liquid water path and droplet concentration. Precipitation liquid water contents differed by almost two orders of magnitude between clouds. A detailed sectional model of the coalescence process is described. The model is initialised using the observed droplet size distributions for radii less than 20 mum and evolves the drop size distribution by solving the stochastic coalescence equation. The effects of droplet recycling through turbulence in cloud are accounted for using a transilient matrix approach and are shown to be very important. The model reproduces relatively well characteristics of the observed drizzle drop size distributions. Drizzle characteristics are highly dependent upon the concentration of droplets in the 15-20 mum radius range.

It is suggested that there exists a maximum liquid water path, increasing with cloud droplet concentration, attainable by stratiform cloud layers in the atmosphere. Regions of clouds exceeding this maximum liquid water path rapidly lose liquid water through drizzle production and assume new lower liquid water path equilibrium states. MAXLWP $/approx$ 7 $N_d^{2/3}$

Keywords: stratocumulus, drizzle production, coalescence, turbulence

1 Introduction

The production of drizzle in warm stratiform clouds is a potentially important climatological process because (a) drizzle droplets are ubiquitous in stratiform boundary layer cloud and (b) stratus/stratocumulus is the dominant cloud type over large areas of the ocean. The effect of drizzle upon the cloud liquid water path, the hydrological cycle and the structure and stability of the boundary layer is not well known because of the difficulty in coupling accurate size-resolved microphysical models with high-resolution dynamical models. There is little doubt that accounting for turbulent redistribution of droplets within boundary layer stratiform clouds is necessary to obtain realistic drizzle precipitation rates (Nicholls 1987, Austin et al. 1995). In the simulations of Nicholls (1987), realistic levels of turbulence were included using a transilient matrix technique (Stull 1984). It was found that the turbulence, by allowing large drops to be maintained for longer within the cloud, vastly increased the concentration of large drops throughout the cloud. Although the turbulence levels in Nicholls' simulations were modest (vertical wind standard deviation 0.09< σ_w <0.72 m s^{-1}). the results suggest that parameterizations of drizzle formation in boundary layer clouds would be incomplete and inaccurate without accounting for the turbulence intensity.

[1] *Corresponding author address*: Dr. Robert Wood, Meteorological Research Flight, Building Y46, DERA, Farnborough, Hampshire, GU14 6TD, UK
Email: robwood@meto.gov.uk

Recent work has suggested other mechanisms for promoting drizzle production. Feingold et al. (1999), used a suite of microphysical and dynamical models, including large-eddy simulations with explicit microphysics, to show that the inclusion of realistic numbers of giant haze particles could increase the amount of drizzle liquid water content. The effect is more marked when the background drizzle rate (the drizzle rate without the inclusion of giant haze particles) is low. For example, in simulations of a 450 m thick stratocumulus cloud with a droplet concentration of 250 cm^{-3}, the addition of 10^{-2} cm^{-3} haze particles with radii of 20 μm increased the drizzle liquid water content by more than an order of magnitude. Such concentrations of large haze particles (which contain predominantly sea-salt) can be produced at the sea surface by whitecapping under high wind speed conditions (Monahan et al. 1986). If the cloud layer is close to the surface then there is a greater chance that these particles will be assimilated into the cloud and take part in the collision-coalescence process. It is important therefore to be able to quantify the magnitude of this effect at different wind speeds.

Another important issue is that the drizzle in stratocumulus clouds tends to occur in intermittent patches (Austin et al. 1995). These patches may occur in regions where the cloud thickness is significantly greater than the mean cloud thickness of the layer as a whole. Thicker regions of cloud will have larger droplets and higher liquid water contents near cloud top than thinner regions and the relationship between cloud thickness and coalescence rate is thought to be strongly nonlinear (Nicholls 1987, Austin et al. 1995). The mean drizzle precipitation rate produced by a cloud with a thickness equal to the mean thickness of the cloud is likely therefore to be lower than the drizzle rate produced by the inhomogeneous cloud. This leads to a biased precipitation rate if, in a GCM, grid-box mean values are used to estimate the precipitation rate (Larson et al. 2000; Wood et al. 2000). We examine the likely magnitude of these biases in this study.

The study is composed of two parts. In part I we describe observations of drizzle in stratocumulus clouds that have been obtained using the Met Office C-130 research aircraft in 12 stratocumulus cloud sheets. Eleven of the flights were flown over the Atlantic Ocean and North Sea around the UK. The other flight examined was flown as part of the ASTEX Lagrangian 1 suite in the Azores region of the Atlantic Ocean. All flights were flown specifically to obtain extensive observations of the vertical structure of the cloud deck. The clouds examined have a considerable variety of droplet concentrations, liquid water paths and drizzle production rates which allows us to make inferences about (a) the role of droplet concentration and liquid water path upon the production of drizzle and (b) the effects of drizzle upon the depletion of liquid water content in stratocumulus clouds. Part II of the study presents a model study of the drizzle formation process in which the observations provide validation for two types of model, which differ considerably in their complexity. The first type of model is a bin microphysical multi-layer model similar to that of Nicholls (1987) and Austin et al. (1995) which takes as inputs the observed cloud droplet size distributions (droplets with radii smaller than 20 microns) and solves the stochastic collection equation at each level to generate an equilibrium drizzle droplet size distribution. The effects of sedimentation, turbulent redistribution, condensational and radiative growth of drizzle droplets are included. The second model type is a much simpler multi-level model in which the drizzle is represented by a single variable (the drizzle liquid water content) at each level. As with the bin-microphysical model, the cloud droplet size distribution is used to initialise the simulations. However, only two moments, the liquid water content and the droplet concentration, are used. The drizzle water content is generated using simple autoconversion and accretion formulations. Sedimentation is simulated using a sedimentation rate-drizzle water content relationship derived from observations. The effects of condensational and radiative cooling growth of drizzle droplets is not included. This type of model is closer to models typically used to model rain growth in large-scale numerical models.

This paper examines the role of turbulence, large haze particles and cloud thickness variability in the production of drizzle within stratocumulus layers. We compare aircraft observations of stratocumulus with results from a 1-D bin microphysical model which includes the effects of turbulent mixing and large sea-salt particle production. By running a number of simulations for each case, we examine the effect of a variable cloud thickness upon the mean precipitation rate. Section 2 presents details of the numerical model formulation. In section 3 aircraft observations are described and presented. In section 4 we present a detailed comparison of the aircraft observations and the numerical model. We conclude our findings in section 5.

2 Case details

(a) Flights

All aircraft data were collected using *The Met. Office* C-130 aircraft in stratus and stratocumulus clouds. Twelve flights are presented in this study. Eleven of the flights took place during the day over the oceanic waters around the United Kingdom. One flight (A209) was flown at night as part of the ASTEX 1st Lagrangian experiment in the Azores region of the Atlantic Ocean. Table 1 presents details of the flight numbers, locations, times, mean cloud base and cloud top height, mean liquid water path, mean droplet concentration and mean cloud base precipitation rate. In this the different cases will be referred to by flight number. There is a considerable range of mean liquid water path (45-360 g m^{-2}), droplet concentration (8-420 cm^{-3}) and precipitation rate (0.046-2.90 mm day^{-1}) between flights which will allow inferences to be made as to the dependence of drizzle formation upon cloud bulk and microphysical parameters.

The sampling strategy differed between flights, although in each case there was good sampling of the vertical and horizontal structure of the cloud. In all flights the mean aircraft position followed an approximately lagrangian path, drifting with the mean wind in the boundary layer (as deduced from real-time aircraft measurements), which limits analysis problems associated with advection. Flights consisted of a series of straight and level runs, in, above and below cloud, together with a number of vertical ascents from above cloud to the surface ($\sim$ 15 m). Many of the flights were augmented with a series of sawtooth runs up and down through the cloud (from approximately 100 m below to 100 m above cloud), to give enhanced vertical sampling of the cloud. The total number of ascents/descents through cloud varied from 3 (A209) to 43 (A693). At least one ascent on each flight characterised the atmosphere from cloud top to $\sim$6000 m. Where possible a run was carried out at the lowest possible flight altitude ($\sim$ 30 m) to characterise the lower boundary conditions. The straight and level runs were typically 60 km in length, but on flights A648 and A649 a greater number of shorter runs were used (20 km). The total length of horizontal flight legs allowed reasonable turbulence statistics to be derived from the data.

(b) Instrumentation and data analysis methods

Instrumentation to measure dynamic (wind components) and thermodynamic (humidity, liquid water content) variables is described in more detail in Rogers et al. (1995). Cloud microphysical measurements were made using a PMS (Particle Measuring Systems) Forward Scattering Spectrometer Probe (FSSP) which counts and sizes particles into 15 size bins in the radius range 1-23.5 μm. Larger particles were measured using a PMS 2D-C optical array probe which counts and sizes particles into 32 size bins in the radius range 12.5-400 μm. For the 2D-C data the first size bin is not used as there is large uncertainty in the sizing of particles in this bin (Korolev et al. 1998). Combined FSSP and 2D-C size distributions are produced by linear interpolation in $\log(dN/dr)$-log(r) coordinates. To facilitate comparison with the model size distributions, the observed spectra are interpolated onto the model radius bins (logarithmically spaced in radius). Sea surface temperature was measured using a Heimann nadir-pointing radiometer and was corrected for absorption between the surface and the lowest flight level using the method of Hignett (????).

Turbulent variance and covariance flux measurements were derived from the data using by first detrending the time series by removing a 3 km wide running mean and then using eddy correlation. This removes effects caused by erroneously drifting sensor outputs and transports caused by motions significantly larger than the largest turbulent eddies.

(c) Case details and overviews

All four flights described in this paper took place over the sea around the UK. Table 1 gives details of the dates and locations, together with some mean properties of the clouds measured. Most of the flights took place between the hours 11 UTC and 16 UTC. It is clear that there is a considerable range of droplet concentrations (25-400 cm^{-3}) and cloud liquid water paths (45-360 g m^{-2}) between the flights. The liquid water paths LWP were calculated using a number of ascents/descents through the cloud layer. This method of estimating liquid water path is prone to bias because the aircraft does not make a vertical passage through cloud, but instead moves with an ascent/descent rate of approximately ± 3 m s^{-1}. For a 300 m deep cloud the horizontal distance travelled between cloud base and cloud top is some 10 km at a science cruising speed 100 m s^{-1}. However, when calculating a mean value of LWP the degree of bias becomes less as the number of ascents increases. We carried out simple tests using a hypothetical cloud with a sinusoidal cloud base height and constant cloud top. This allowed us to estimate the degree of uncertainty in our estimated value of $\overline{LWP}$. Droplet concentration is measured using the Forward Scattering Spectrometer Probe (FSSP, see e.g. Baumgardner et al. 1993). The number of droplets with sizes larger than the maximum measurable by the FSSP (23 μm radius) does not contribute significantly to the total in-cloud droplet concentration in any of the cases. We calculate the mean droplet concentration using all 10 second samples in the height range $0.33 < z_* < 0.67$ to avoid sampling regions close to cloud base and cloud top. The error in the mean is then $\sigma_{N_d}/sqrt(N)$ where N is the number of samples. For all flights this error is very small (< 5 cm^{-3}).

Also given in Table 1 is the mean cloud base precipitation rate. We define z_* as a normalised height given by

$$z_* = \frac{z - \overline{z_{CB}}}{\overline{z_i} - \overline{z_{CB}}} \tag{1}$$

where $\overline{z_{CB}}$ and $\overline{z_i}$ are the mean cloud base height and cloud top respectively and z is the height of a particular measurement. Because it is not possible to assign a local cloud base to every measurement, it is possible due to the spatial and temporal variability in the cloud geometrical properties that a measurement at height z could be either above or below cloud base when $z_* = 0$. We calculate the cloud base precipitation rate as being the average precipitation rate in the region $0 < z_* < 1/3$. For a given cloud particle size distribution, the precipitation rate P is calculated from

$$P = \frac{4}{3}\pi\rho_w \int_{r=0}^{\infty} w_T(r)\frac{dn}{dr}r^3 dr \tag{2}$$

where $w_T(r)$ is the terminal velocity of a droplet of radius r, $\frac{dn}{dr}$ is the number of droplets in the size range r to $r + dr$, and ρ_w is the density of liquid water. Values of w_T as a function of size are calculated using the Reynold's number-Best number method as described in Pruppacher and Klett (1997). We calculate P only over the radius range $20 < r < 400\mu$m. There were no drops measured larger than 400μm. Interestingly, droplets smaller than 20 μm can contribute considerably to the precipitation rate, but the fall speeds are so small ($w_T \approx 5$ cm s^{-1} for $r = 20\mu$m falling to just over 1 cm s^{-1} for $r = 10\mu$m) that it would take 8 hours for a 10

μm droplet to fall through a 300 m thick cloud. Turbulent effects therefore are much more important at determining the trajectories of droplets smaller than $\sim$ 20 μm.

Dynamic and thermodynamic parameters for the cases are given in Table 3. The SST was calculated from a run at the lowest flight level. Typical errors are of the order 0.4 K. The wind speed U_{10} at a height of 10 m is estimated using the mean wind speed at the lowest flight level (100 m in all cases) and extrapolating this measurement down using a logarithmic wind profile (e.g. Bretherton et al. 1995) and a roughness length of 5×10^{-4} m (suitable for oceanic conditions, Stull 1988). The friction velocity is estimated using the u and v momentum fluxes from the lowest flight leg ($\sim$ 30 m in all cases). The friction velocity scales quite well with U_{10} using the Charnock (1955) relation with $c = 11.0$ (see Nicholls and Readings 1979), apart from at low wind speed ($U_{10} < 3$ m s^{-1}) where the observed friction velocities exceed those from Charnock's relation. The convective velocity scale w_* is calculated using the buoyancy integral method (e.g. Deardorff 1980) as described in Nicholls and Leighton (1986). We use the bouyancy integral over the entire boundary layer from the surface to cloud top. In some cases the buoyancy integral was negative due to low buoyancy generation in cloud or because the air was being cooled by a lower SST so that negative subcloud virtual potential temperature fluxes were produced. In these cases the w_* could not be defined. Turbulent kinetic energy (TKE) in the boundary layer is generated by buoyant generation, shear generation or a mixture of the two. In boundary layers driven predominantly by shear generation observations suggest that the vertical wind variance scales well with u_* (see e.g. Nicholls and Leighton 1986) and we also find this for cases A644, A648 and A762. A measure of the relative roles of shear and surface buoyancy production of TKE is given by the ratio of the boundary layer depth z_i to the Monin-Obukhov length L_{MO}. Large positive values of $-z_i/L_{MO}$ indicate that turbulence is driven primarily by thermal convection. Small negative values that shear generation of turbulence dominates. Our definition of L_{MO} accounts for the fact that cloud top cooling in addition to surface forcing can be an important source of buoyancy generation, so we define as

$$L_{MO} = -z_i \frac{k w_*^3}{u_*^3} \tag{3}$$

where $k = 0.4$ is the Von Karman constant, and w_* is defined using the buoyancy integral as mentioned above. Positive values of L_{MO} are possible because the bouyancy integral can be negative. Table 3 shows that flights A049, A209, A439, A641, A649, A764 and A767 are all dominated by buoyancy generation, with the other flights being driven primarily by shear production.

Also presented are the mean in-cloud vertical wind standard deviation $\overline{\sigma_w}$, which tends to be larger in the convectively driven cases. To assess the role of radiation in generating cloud turbulence we simulate radiative transfer through the clouds using a four-stream radiative code (Edwards and Slingo, ref???). Long-wave flux divergences across the boundary layer as shown in Table **??** are all negative (net loss) and range from around -50 W m^{-2} in cases with relative cold cloud tops and moist lower tropospheres, to -85 W m^{-2} in summer cases with low moisture above the boundary layer. In contrast, the short-wave flux divergences are strongly modulated by the solar zenith angle. Because all of the flights were flown at approximately the same local time each day (apart from A209 which was at night), this results in a strong winter-summer difference in short-wave flux divergence, with relatively little absorption for the winter cases (maximum 21 W m-2) to values comparable to, or even greater than the magnitude of the long-wave flux divergence. For all the winter cases this results in a net loss of radiation of 30-45 W m^{-2}. The net gain/loss in the daytime summer cases is much smaller (net losses between -7 to 24 W m^{-2}).

Both long-wave cooling rates and short-wave heating rates are largest at cloud top but the decay distance is much smaller for the long-wave cooling rates which results in a sharp net cooling from the cloud top to a few tens of metres below cloud top and a weaker warming through the remainder of the cloud. Because the cloud base temperature is generally colder than the surface temperature, there is a small additional long-wave heating close to the base of the cloud. This warming/cooling profile can destabilise the cloud layer (refs???) and through effects upon the vertical distribution of the sensible heat flux can lead to a decoupling of the cloud layer from the surface. Only two cases had cloud layers that were clearly decoupled from the surface layer (A649 and A767). The reasons for decoupling in A649 (with a mixed layer base at $z \approx$ 200m) are difficult to determine but in A767 a high surface latent heat flux (110 W m^{-2}) was promoting a warming-deepening form of the decoupling (Wyant and Bretherton 1997) as the air mass had moved southwards from the Arctic over the previous two days. Cumulus clouds were observed to form at the top of the surface layer ($\approx$ 600m) and in places penetrated the overlying stratocumulus layer. The other summer case boundary layers remained coupled because of the shallow boundary layers.

The cloud and boundary layer observed in cases A644 and A648 were markedly different in nature to the other cases. Both cases were formed in moist airmasses moving northeastwards from the Azores region over colder seas. The surface heat fluxes in these cases were negative and a shallow (200 m deep) shear-driven mixed layer was present. Above this layer the temperature exhibited a stable lapse rate (2-3 K km^{-1}) up to around 800-1000 m. Patchy layers of cloud were present at most levels in this layer. Above this layer the temperature profiles indicate a moist adiabatic lapse rate which contained less cloud than the stable layer below. This layer was capped with a weak inversion (1-3 K) at 1800-2000 m (A644) and 1400-1600 m (A648) with layer cloud beneath. Back-trajectories calculated using the Met Office NAME trajectory model (ref???) suggested that the lower tropospheric air had been subjected to large-scale ascent in the 24 hour period prior to the observations taken on flights A644 and A648. This ascent was most likely associated with warm frontal zones which, although the surface fronts were analysed as being at least 100-200 km from the observational area, appeared to have a marked affect upon the boundary layer. There were no high or mid level clouds during A644 and some patchy altocumulus layers during A648. The ascent rates for the 24 hour period prior to the observations were estimated as 0.9 and 0.8 cm s^{-1} for A644 and A648 respectively, although the trajectories suggested no large-scale ascent on A644 during the observational period, and subsidence during the observational period on A648.

The mean in-cloud vertical wind integral scale $\overline{\lambda_w}$ is calculated using the autocorrelation method of Lenschow and Stankov (1986). This is a measure of the horizontal distance over which the vertical wind decorrelates, so that large values indicate that large coherent eddies are dominant. Typically in a convective boundary layer this integral scale tends to be smallest at the surface increasing with height. We find this to be the case here. The mean in-cloud integral scale tends to be smallest in clouds capping shallow boundary layers (A693, A763 and A764 all have cloud tops lower than 500 m and $\overline{\lambda_w}$ <100 m) especially when the mixing in the boundary layer is driven largely by shear.

3 Vertical thermodynamic, cloud liquid water and microphysical structure

(a) Temperature and total water content

Figure **??** profiles of mean temperature (a) and total water content (b) in the cloud layer. The temperature is referenced to the moist adiabatic temperature calculated which is calculated using the mean value of the moist adiabatic lapse rate in the cloud layer. The height variation of the moist adiabatic lapse rate from the mean value does not exceed 0.2 K km^{-1} in any of the cases and in most of the clouds it is less than 0.1 K km^{-1}. The data show that the temperature lapse rate in cloud in all cases except A644 and A648 is close to the moist adiabatic rate, which one would expect in the case of a well-mixed boundary layer where the entrainment rate is small ($w_e/w_* \ll 1$). The Rosemount E102AL total temperature sensor used on the C-130 measures air temperature with an error of approximately 0.2-0.5 K. Coupled with the additional problems of possible sensor wetting in cloud , the overall uncertainty in temperature is too large to determine deviations from adiabaticity in the well-mixed cases except close to cloud top where the effects of entrainment are seen. The deviations in A644 and A648 are significant and highlight the considerable subadiabaticity and poor mixing in these cases.

The total water content is plotted as the mean value at each level minus the mean value for the entire cloud layer q_{T*} to facilitate comparison between cases. As with temperature all cases except A644 and A648 show small gradients in total water content with height. In cases A644 and A648 the total water content falls considerably over the height of the cloud. Low in these clouds turbulence caused by shear (in both cases $U_{10} > 9$ m s^{-1}) is transporting moisture laden air upwards. Higher in the cloud the moisture fluxes are small and insufficient to prevent loss of water through drizzle.

(b) Liquid water content and droplet concentration

Drizzle production is strongly dependent upon the liquid water and microphysical cloud characteristics. To facilitate the comparison between flights we define N_* as the mean droplet concentration from all the 1 Hz samples in cloud. A sample is denoted as cloudy if the LWC measured with the Johnson-Williams (JW) hotwire probe exceeds 0.02 g m^{-3}. We choose this threshold to avoid misclassification because the JW probe is known to suffer small instrumentally-related oscillations with an amplitude of between 0.005 and 0.02 g m^{-3} even when the probe is out of cloud. In any case, we found that variation of this threshold between 0.02 and 0.05 g m^{-3} made litte difference to the derived value of N_*. These values are given in Table 1. We then calculate layer averages over a number of height bins (between 8 and 15 depending upon the vertical resolution of the measurements which differed between flights) in the range $0 < z_* < 1$. Figure **??**(a) shows the mean droplet concentration at each height bin normalised with N_* plotted as a function of z_* for each flight. Cases other than A644 and A648 all show a similar behaviour with $\overline{N_d}/N_*$ increasing with normalised height up to around z_*=0.3-0.4 then remaining approximately constant and unity up to z_*=0.8. Above this height the droplet concentrations decrease. Although it is tempting to ascribe the drop-off in droplet concentration and the cloud base and cloud top to effects of nucleation and entrainment respectively, it is important to stress that fluctuations in cloud base and cloud top heights are more responsible for the smaller means near the cloud boundaries. Means calculated using only in-cloud values show near-unity values from very close to cloud base to $z_* \approx 0.9$. Figure **??**(b) shows the standard deviation of the droplet concentration at each height normalised with the mean value at that height. Higher values are found close to the cloud boundaries due to the averaging over both cloudy and clear regions. In the cloud centre values of $\sigma_{N_d}/\overline{N_d}$ are typically 0.1-0.4 for the classical cases. These values can be compared with observations by Noonkester et al. (1984) who found that $\sigma_{N_d}/\overline{N_d}$ between 0.1 and 0.2 in the cloud interior for two stratocumulus case, and increasing values towards the cloud boundaries. Large eddy simulation (Stevens et al. 1996) of a non-precipitating stratocumulus cloud led to values of $\sigma_{N_d}/\overline{N_d}$ of approximately 0.2-0.4 in the central 50% of the cloud increasing to 0.6-1.0 close to cloud base and cloud top. In contrast, the cases A644 and A648 show larger values through much of the cloud layer reflecting the broken nature of the these layers.

Nicholls and Leighton (1986) point out that deviations of a cloud layer from the adiabatic are more easily observed by looking at deviations in liquid water content from adiabatic than by looking at temperature or total moisture. We use the same formulation as Nicholls and Leighton (1986) in that we define a value $q_{ad}(z_i)$ to be the adiabatic liquid water content at cloud top, i.e. $q_{ad}(z_i) = \Gamma_{ad}(\overline{z_i} - \overline{z_{CB}})$ where $\Gamma_{ad}(T, p)$ is the adiabatic increase in liquid water content with height, a weak function of temperature and pressure. A single value of Γ_{ad} is used in each case, calculated using the mean in-cloud temperature and pressure. We then calculate the degree of subadiabaticity by calculating q_{ad} for each level, subtracting the observed mean value $\overline{q_L}$ and normalising with $q_{ad}(z_i)$. This parameter (Fig. **??**(c)) is zero for a fully adiabatic cloud and equal to z_* for cloud free conditions. The clouds range from close to adiabatic (A648) to very subadiabatic (A644, A648) with a broad range in between. Parameters that can affect the degree of adiabaticity are drizzle loss (Stephens et al. 1998) and the balance between the transport of moisture through the cloud boundaries and the efficiency with which turbulent motions can redistribute the moisture through the layer (Wyngaard and Brost 1984, Nicholls and Leighton 1986). Finally, Fig. **??**(d) shows the ratio of the standard deviation of the liquid water content to the mean in the layer as a function of normalised height. This typically decreases through the lowest 2/3 of the cloud before increasing again as the upper boundary is reached.

All clouds with the exception of A641 have distinctly subadiabatic liquid water contents throughout most of the cloud layer. The cases A644 and A648 are highly subadiabatic. The effects of a variable cloud top and entrainment on mean liquid water contents can be seen above $z_* = 0.8$ where the gradient of $(q_{ad} - q_L)/q_{ad}(z_i)$ increases considerably. For most of the cases the gradient in the range $0.2 < z_* < 0.8$, away from the cloud base and top, is approximately constant which indicates that the ratio of the liquid water content at a level to the adiabatic value at that level is constant. Note that a rate of change with normalised height in $(q_{ad} - q_L)/q_{ad}(z_i)$ of 0.4 is equivalent to a difference in total water content across the cloud layer of only around 0.1-0.3 g kg^{-3}, which is close to the accuracy of the total water probe.

Values of $\sigma_{q_L}/\overline{q_L}$ (Fig. **??**(d)) decrease from between 0.5-1.5 close to cloud boundaries in the well-mixed cases to 0.2-0.5 in the cloud interior, similar to the LES simulations of Stevens et al. (1996). Much of this variation reflects the horizontally varying cloud base height rather than variations in the degree of adiabaticity from region to region. This can be deduced by considering the horizontal variation in q_L that one would expect given a particular variation in cloud base. We discuss this further in section ????.

We carried out a more detailed study of the subadiabatic nature of the clouds by looking at each profile individually. In this way, effects of fluctuations in cloud base and top, which contaminate the profiles in Fig. 3 near the cloud boundaries, are reduced. For each profile we estimate cloud base and height from both the droplet concentration measurements and the liquid water content measurement. The two estimates of the cloud boundaries we found to be within 20 m in 85% of cases and within 50 m in all cases. We then calculate the adiabatic liquid water path for each profile as $LWP_{ad} = (1/2)\Gamma_{ad}(z_i - z_{CB})^2$, where Γ_{ad} is calculated using the mean temperature and pressure in the cloud layer. We estimate the liquid water path from the observed profile by simple integration of the observed q_L. The ratio f_{ad} of the observed to adiabatic LWP is thus estimated for each profile. The mean of these values for each flight is given in Table 2. We estimate the error in mean LWP using profiles through a hypothetical cloud where the local liquid water content is a linear function of height above the local cloud base. The cloud has a sinusoidal cloud base and flat cloud top. The amplitude of the sinusoid is taken from the observations of cloud base height. The horizontal wavelength is taken to be 20-40 km, a typical lengthscale for cloud base fluctuations in stratocumulus clouds. Each individual profile can result in a biased LWP because of variations in cloud base. Given enough profiles for each case this method results in an unbiased estimate of the cloud LWP and f_{ad}. The errors increase as the horizontal wavelength increases and decrease as the number of profiles increases. The error in f_{ad} is shown in Table 2. This error does not include unknown systematic errors in the JW liquid water content sensor used to make the measurements, but these are likely to be smaller than 10%.

Figure 4 shows for two cases (A641 - 20 profiles; A763 - 25 profiles) the mean ratio q_L/q_{ad} of observed to adiabatic liquid water content as a function of normalised height using the individual profile method. Both cases show a near-constant value of of adiabaticity through the bulk of the cloud ($0.2 < z_* < 0.9$) with a fall-off due to entrainment for $z_* > 0.9$. Values close to cloud base are more prone to error because of the small values of liquid water content there. The results suggest that the cloud in A641 is almost completely adiabatic and that the liquid water content in A763 is roughly 60-70% of adiabatic. This is reasonably consistent with the values in Fig. 3 which show normalised height gradients of $d((q_{ad} - q_L)/q_{ad}(z_i)/dz_*$ of ≈ 0 and ≈ 0.4 respectively in the bulk of the cloud (note that $q_L/q_{ad} = 1.0 - d((q_{ad} - q_L)/q_{ad}(z_i)/dz_*)$. We are fairly confident about adiabaticity values in most of the clouds (see estimated errors in Table 2), but the cause of the variability among the different cases is more difficult to pin down, and we discuss this further in section (???).

(c) Cloud fraction

Figure 5 shows the cloud fraction as a function of normalised height for all the cases. Cloud fraction in all cases except A644 and A648 is obtained from the 1Hz FSSP droplet concentration using a threshold of 5 cm^{-3} to define the presence of cloud (Wood and Field (2000)). This threshold concentration is appropriate because it is several times higher than the highest super-micron aerosol concentrations but also substantially smaller than typical cloud droplet concentrations. Because the droplet concentrations in A644 and A648 were in places very low (¡ 10 cm^{-3}) we chose to use the JW liquid water content with a threshold of 0.02 g kg^{-1}. We chose the FSSP over the JW in the other cases because of its faster response time.

In all the well-mixed cases there is near total cloud cover (cloud fraction ¿ 0.9) in the range $0.3 < z_* < 0.8$ with a drop-off to 0.4-0.8 at the mean cloud base and top. The cases A644 and A648 show less than total cloud cover at all levels. The largest cloud fractions (0.6-0.8) in these cases are found at $z_* < 0.5$, a minimum in cloud fraction at occurs at intermediate levels, and a second peak in cloud fraction is observed around $z_* = 0.8 - 0.9$. It is interesting that the frontal cases both show a two-layer cloud structure. Very low accumulation-mode aerosol concentrations (10-20 cm^{-3}) were observed in the clear region between the layers and above cloud in both cases, suggesting that depletion of aerosol through heavy drizzle may be rendering the upper cloud deck colloidally unstable. Large eddy simulations of the A648 case (Wood, Ghosh and Jonas 2001) show that the lower cloud layer may have resulted from the moistening and cooling of the boundary layer caused by evaporating drizzle from the upper level. That a two-layer structure is observed in both frontal cases could suggest that the responsible processes could be a common feature of warm, clean stratus in ascent regions close to fronts.

(d) Vertical wind

The vertical wind standard deviation σ_w is important for mixing in the cloud. Figure 6(a) shows profiles of σ_w as a function of normalised height in cloud for the different cases. In the buoyancy-driven cases this is relatively constant with height in the cloud layer. Shear-driven cases particularly A762, A644 and A648 show a general decrease in σ_w with height reflecting that the turbulence is driven primarily by surface friction. Figure 6(b) shows profiles of the vertical wind integral scale, which varies considerably between cases, and also with height in some of the cases. Lenschow and Stankov (1986) find that in convective boundary layers driven by surface heating the integral scale increases with height away from the surface. Clearly it seems reasonably intuitive to find eddy sizes becoming smaller towards fixed boundaries. However, for turbulence generated near cloud top as in the case of radiatively driven stratocumulus, the inversion does not impose a rigid lid to the turbulent eddies, although one would suspect it to dampen considerably the larger eddies resulting in smaller integral scales. However, short-wavelength gravity waves that may occur in the stable inversion layer cannot be distinguished from turbulent eddies when deriving integral scale using autocorrelation, it is unclear what we would expect. Our results do not appear to show any consistent height trends in the integral scale. [Compare with other measurements in Sc]. As noted in section ??? shear-driven turbulence generally results in smaller eddies.

Vertical wind standard deviation has been shown to be important in the production of drizzle (Nicholls 1987; Austin et al. 1995). Stronger turbulence can increase the recycling of drizzle drops in thin cloud layers resulting in huge increases in the number of large drizzle drops. This will have important consequences for the evaporation rates below cloud and in determining how much of the precipitation present at cloud base will reach the surface. The integral scale can also have considerable consequences for the transport of drizzle drops in cloud. Smaller eddies result in slower plume broadening which for falling droplets may result in less efficient recycling. We examine the effects of turbulence further in part II.

(e) Drop size distributions

All cases contain drizzle-sized droplets, in this study defined as droplets with radii larger than 20 μm. We choose this size as a partition as it represents the crossover radius where, at typical supersaturations found in boundary layer clouds, condensation growth, the dominant process for the growth of small cloud droplets, becomes less effective than growth by coalescence (e.g. Jonas 1996). Precipition rates in 2-3 km thick warm Hawaiian rainband clouds can be as high as 20 mm hr^{-1}. At these rates the effect of precipitation has a marked effect upon cloud dynamics and structure through evaporative cooling below cloud base and depletion of cloud water. What is much less clear is the effect that precipitation has upon the dynamics of shallower stratocumulus clouds. Jensen et al. (2000) present observational evidence that evaporation of drizzle patches can generate cold microfronts akin to, albeit much weaker than, microburst density currents from thunderstorms. Jensen et al. showed that in a stratocumulus/cumulus case in the Southern Ocean the density current caused a local convergence region and spawned the generation of cumulus clouds beneath the stratiform deck which led to a thickening of the cloud. In a large eddy modelling study of shallow stratocumulus with heavy drizzle Stevens et al. (1998) showed a transition towards more cumulus-type circulations in the boundary layer, with weakened entrainment and depleted liquid water path.

Observations of cloud droplet ($r < 25\mu$m) size distributions in warm stratiform cloud are quite common in the literature (e.g. Noonkester, Nicholls, Liu, Boers et al. Martin et al. 1994; Brenguier 2000; Wood et al. 2001) to the point where they now form an active area of parameterisation research. Fewer detailed cases of observations of drizzle size distributions are to be found however, but there are a number of detailed studies (e.g. Nicholls; Boers et al 1996; Wood et al. 2001). Mention some more about the findings.

In general, observations of drizzle in stratocumulus clouds show that the droplet size distributions for drops larger than around 20 μm broaden towards clouds base. This is because drizzle drops form in the upper levels of the cloud, where the cloud droplets growing through condensation are largest, through the coalescence of cloud drops. These drops then fall through cloud growing larger by collecting other drizzle and cloud drops. Figure 7 shows some of the characteristics of the populations of drizzle droplets ($r > 20\mu$m) at different levels in cloud. Drizzle droplet concentrations $N_{d,D}$, liquid water contents $q_{L,D}$ and precipitations rates P are all normalised with their respective in-cloud means, which are given in Table 4.

4 Cloud horizontal variability

The ratio of the standard deviation to mean cloud liquid water content and droplet concentration were presented as a function of height in Fig **??**. A simple model of the cloud relates the in-cloud liquid water content variability to variability in cloud base height, assuming a constant value for the rate of increase in liquid water content with height above the local cloud base (Considine et al. 1997). Observations have shown that in many cases this provides a reasonably accurate model of cloud liquid water content variability. The model predicts that the standard deviation of liquid water content σ_{q_L} at a level entirely in cloud can be given by

$$\sigma_{q_L} = \Gamma_{eff}\sigma_{z_{CB}} \tag{4}$$

where $\sigma_{z_{CB}}$ is the standard deviation of cloud base height and Γ_{eff} is the rate of increase in liquid water content with height. It is not necessary that Γ_{eff} is the adiabatic value Γ_{ad}, only that it is constant for a particular cloud. Many of the flights here contained quite an unusually large number of profiles through cloud which allows a relatively accurate measure of the cloud base height variability.

With data taken from the profiles shown in Fig. **??** we plot the mean value of σ_{q_L} at cloud centre $(0.4 < z_* < 0.6)$ against the standard deviation of cloud base height in all the cases with more than 10 profiles.

Table 1: Flight numbers, dates, locations, times, cloud type, mean heights of cloud base $\overline{z_{CB}}$ and cloud top ($\overline{z_i}$), mean liquid water path $\overline{LWP}$ ($\pm$ error), mean in-cloud droplet concentration N_* and mean cloud base precipitation rate P_{CB}. Note that the errors are errors in the mean value rather and not estimates of the variability in that parameter.

Flight	Date	Location	Time [local]	Type	$\overline{z_{CB}}$ [m]	$\overline{z_i}$ [m]	$\overline{LWP}$ [g m^{-2}]	N_* [cm^{-3}]	P_{CB} [mm d^{-1}]
A049	6 Dec 90	SW App.	12-15	Sc	825±23	1450±34	260±44	310	0.49
A209	12 Jun 92	Azores	00-04	Sc	310±44	705±27	170±34	120	0.47
A439	29 Feb 96	NW Ireland	12-15	Sc	780±19	1150±9	100±15	90	0.24
A641	3 Dec 98	S. North Sea	11-16	Sc	430±7	1110±14	360±16	420	0.054
A644	14 Dec 98	SW App.	12-15	St	150±75	1800[1]	90±50	20	0.66
A648	28 Jan 99	SW App.	12-15	St	190±18	1550[1]	85±50	8	1.12
A649	29 Jan 99	SW App.	12-16	Sc	450±9	775±13	80±6	60	0.095
A693	8 Jul 99	NW Ireland	12-16	St/Sc	115±21	395±3	80±3	110	0.41
A762	12 Jun 00	SW App.	12-16	St/Sc	180±13	495±11	80±5	95	0.28
A763	14 Jun 00	SW App.	12-16	St/Sc	245±18	485±14	45±2	85	0.34
A764	15 Jun 00	SW App.	12-16	St/Sc	≈20[2]	320±6	70±6	65	0.44
A767	28 Jun 00	North Sea	12-15	Sc w/Cu	935±24	1350±10	90±10	110	0.78

Notes: 1. The cloud consisted of two or more layers which were heterogeneous and often had indistinct vertical boundaries. The figure for mean cloud top given is for the uppermost layer. 2. The aircraft was not able to descend to cloud base due to visibility restrictions. This cloud base was estimated by extrapolation of the profiles of liquid water content from higher levels.

Figure captions

Figure 1. Profiles of (a) temperature; (b) total water content; (c) liquid water content (line) and cloud fraction (circles); (d) droplet concentration for flight A644. In (a), (b) and (c) circles represent run means from 60 km horizontal runs.

Table 2: Values of mean in-cloud total water content q_*, cloud base pressure p_{CB}, temperature T_{CB} and ratio of observed to adiabatic liquid water path f_{ad}. The error in f_{ad}, given at the 1-σ level, is estimated using a simple model of cloud structure (see text).

Case	q_* [g kg^{-1}]	p_{CB} [hPa]	T_{CB} [K]	f_{ad}
A049	5.1	928	275.5	0.60 $\pm$ 0.10
A209	10.1	987	287.3	0.92 $\pm$ 0.18
A439	4.6	940	273.9	0.77 $\pm$ 0.08
A641	3.1	960	270.7	0.99 $\pm$ 0.04
A644	8.4	996	285.1	0.08 $\pm$ 0.09
A648	6.6	993	282.0	0.14 $\pm$ 0.08
A649	6.6	972	279.7	0.72 $\pm$ 0.05
A693	9.6	1005	286.0	0.77 $\pm$ 0.03
A762	9.4	998	286.0	0.67 $\pm$ 0.04
A763	9.2	993	285.7	0.67 $\pm$ 0.02
A764	8.9	1011	285.0	0.59 $\pm$ 0.05
A767	4.8	909	274.6	0.64 $\pm$ 0.07

Table 3: Thermodynamic and dynamic details of the cases studied. From left to right: sea surface temperature SST; 10 metre wind speed U_{10}; friction velocity u_*; mean in-cloud value of the vertical wind speed standard deviation $\overline{\sigma_w}$; mean in-cloud vertical wind integral scale $\overline{\lambda_w}$; ratio of inversion height to the Monin Obukhov length -z_i/L_{MO}; mean inversion jump in virtual potential temperature $\Delta\theta_v$; mean inversion jump in total water content Δq_T.

Case	SST [K]	U_{10} [m s^{-1}]	u_* [m s^{-1}]	w_* [m s^{-1}]	$\overline{\sigma_w}$ [m s^{-1}]	$\overline{\lambda_w}$ [m]	-z_i/L_{MO} [m]	$\Delta\theta_v$ [K]	Δq_T [g kg^{-1}]
A049	283.3	5.1	0.19	0.63	0.58	175	14.6	5.7	-2.0
A209	290.3	8.1	0.26		0.70	150		2.9	-1.0
A439	281.6	6.2	0.25	0.89	0.59	130	18.0	5.5	-3.6
A641	282.5	0.7	0.13	0.97	0.65	230	166	4.3	-0.5
A644	284.7	9.7	0.47	-	0.37	200	-0.50	n/a[1]	n/a[1]
A648	283.9	13.3	0.37	0.33	0.25	200	0.28	n/a[1]	n/a[1]
A649	283.6	2.2	0.14	0.62	0.28	180	34.8	2.7	-1.1
A693	286.4	10.7	0.34	0.43	0.38	35	0.81	5.4	-0.8
A762	286.5	11.3	0.40	-	0.30	60	-0.27	4.4	-0.9
A763	287.2	7.3	0.18	-	0.26	160	-0.84	4.8	-0.3
A764	287.7	1.3	0.14	0.44	0.28	80	12.4	2.3	-0.5
A767	285.1	10.1	0.38	0.95	0.50	130	6.25	3.6	-2.7

[1] These cases contained multiple weak inversions ($\Delta\theta_v < 1$ K; $\Delta q_T < 0.5$ g kg^{-1}) both in and above the cloud layers and it is therefore not possible to define a good measure of the inversion jumps.

Table 4: In-cloud mean drizzle drop concentration $\overline{N_{d,D}}$, liquid water content $\overline{q_{L,D}}$ and precipitation rate $\overline{P}$. Also given are cloud top ($0.8 < z_* < 1.0$) and cloud base ($0.0 < z_* < 0.2$) values of the drizzle drop volume radius $r_{v,D}$

Case	$\overline{N_{d,D}}$	$\overline{q_{L,D}}$	$\overline{P}$	$r_{v,D}$ (base)	$r_{v,D}$ (top)
	[l^{-1}]	[10^{-3} g m^{-3}]	[mm day^{-1}]	[μm]	[μm]
A049	37	11.3	0.51	53	38
A209	60	11.2	0.39	46	29
A439	30	7.5	0.26	45	35
A641	18	2.2	0.08	31	29
A644	59	20.9	0.99	42	43
A648	147	30.9	0.80	53	32
A649	46	6.8	0.17	38	30
A693	135	17.6	0.32	37	28
A762	170	17.7	0.28	36	26
A763	118	15.3	0.27	39	27
A764	89	21.8	0.58	44	35
A767	141	21.0	0.67	53	25

5 References

Austin, P., Wang, Y., Pincus, R. and Kujala, V., 1995a. Precipitation in stratocumulus clouds: observations and modelling results. *J. Atmos. Sci.*, **52**, 2329-2352.

Austin, P, Siems, S. and Wang, Y., 1995b. Constraints on droplet growth in radiatively cooled stratocumulus clouds. *J. Geophys. Res.*, **100**, D7, 14231–14242.

Berry E. X. and Reinhardt, R. L., 1974. An analysis of cloud droplet growth by collection. Part I: Double distributions. *J. Atmos. Sci.*, **31**, 1814-1824.

Bott, A., 1989. A positive definite advection scheme obtained by nonlinear renormalization of the advective fluxes. *Mon. Wea. Rev.*, **117**, 1006-2636.

Bott, A., 1998. A flux method for the numerical solution of the stochastic collection equation. *J. Atmos. Sci.*, **55**, 2284-2293.

Bretherton, C. S., Austin, P. and Siems, S. T., 1995. Cloudiness and marine boundary layer dynamics in the ASTEX Lagrangian Experiments. Part II: Cloudiness, drizzle, surface fluxes and entrainment. *J. Atmos. Sci.*, **52**, 2724-2735.

Cooper, W. A., 1989. Effects of variable growth histories on droplet size distributions. Part I: Theory. *J. Atmos. Sci.*, **46**, 1301–1311.

Davis, M. H., 1972. Collisions of small droplets: Gas kinetic effects. *J. Atmos. Sci.*, **29**, 911-915.

Edwards, J. M. and Slingo, A., 1996. Studies with a flexible new radiation code. I: Choosing a configuration for a large-scale model. *Quart. J. Roy. Meteorol. Soc.*, **122**, 689–720.

Feingold, G., Cotton, W. R., Kreidenweis, S. M. and Davis, J. T., 1999. The impact of giant cloud condensation nuclei on drizzle formation in stratocumulus: implications for cloud radiative properties. *J. Atmos. Sci.*, **56**, 4100-4117.

Golovin, A. M., 1963. The solution of the coagulation equation fro cloud droplets in a rising air current. *Izv. Akad. Nauk. SSSR. Ser. Geofiz.*, **5**, 783-791.

Gong, S. L. and Barrie, L. A., 1997. Modeling sea-salt aerosols in the atmosphere. 1: Model development. *J. Geophys. Res.*, **102**, 3805-3818.

Hall, W. D., 1980. A detailed microphysical model within a two-dimensional dynamic framework: Model description and preliminary results. *J. Atmos. Sci.*, **37**, 2486-2507.

Hunt, J. C. R., 1981. Diffusion in the SBL. *Atmospheric turbulence and air pollution modelling: A course held in the Hague*, 21-25 September 1981, F. Nieuwstadt and H. van Dop, Eds, D Reidel, 231-274.

Jonas, P. R., 1972. The collision efficiency of small drops. *Quart. J. Roy. Meteorol. Soc.*, **98**, 681-683.

Korolev, A. V., Strapp, J. W. and Isaac, G. A., 1998. Evaluation of the accuracy of PMS Optical Array probes. *J. Atmos. Oceanic Technol.*, **15**, 708-720.

Laird, N. F., Ochs III, H. T., Rauber, R. M. and Jay Miller, L., 1998 Microphysical properties of Florida small cumulus clouds. Part I: Observations. *Proceedings of AMS Conference on Cloud Physics*, 486-489, 17-21 August 1998, Everett, USA.

Monahan E. C., Spiel, D. E. and Davidson, K. L., 1986 A model of marine aerosol generation via whitecaps and wave disruption. In *Oceanic Whitecaps*, edited by E. C. Monahan and G. Mac Niocaill, 167-174, D. Riedel, Norwell, Mass., USA

Nicholls, S. and Leighton, J., 1986 An observational study of the structure of stratiform cloud sheets: Part 1. Structure. *Quart. J. Roy. Meteorol. Soc.*, **112), 431–460.**

Nicholls, S., 1987. A model of drizzle growth in warm, turbulent, stratiform clouds. *Quart. J. Roy. Meteorol. Soc.*, 113, 1141-1170.

O'Dowd, C. D. and Smith, M. H., 1993. Physicochemical properties of aerosol over the Northeast Atlantic: Eivdence for wind-speed-related submicron sea-salt aerosol production. *J. Geophys. Res.*, 98, 1137-1149.

Politovich, M. K. and Cooper, W. A., 1988. Variability of the supersaturation in cumulus clouds. *J. Atmos. Sci.*, 45, 1651–1664.

Rogers, R. R. and Yau, M. K., 1989. *A short course in cloud physics.* **Third edition, Pergamon Press, Oxford, UK.**

Rogers, D. P., Johnson, D. W. and Friehe, C. A., 1995. The stable internal boundary layer over a coastal sea. Part I: Airborne measurements of the mean and turbulence structure. *J. Atmos. Sci.*, 52, 667-683.

Stevens, B., Feingold, G., Cotton, W. R. and Walko, R. L., 1998. Elements of the microphysical structure of numerically simulated nonprecipitating stratocu-

mulus. *J. Atmos. Sci.*, 53, 980–1006.

Stull, R. B., 1984. Transilient turbulence theory. Part I: The concept of eddy-mixing across finite distances. *J. Atmos. Sci.*, 41, 3351-3367.

Stull, R. B. and Hasegawa, T., 1984. Transilient turbulence theory. Part II: Turbulent adjustment. *J. Atmos. Sci.*, 41, 3368-3379.

Stull, R. B., 1988. *An introduction to boundary layer meteorology.* Kluwer Academic Publishers, Dordrecht, The Netherlands.

Wood, R., 2000. Parametrization of the effect of drizzle upon the droplet effective radius in stratocumulus clouds. *Quart. J. Roy. Meteorol. Soc.*, 126, 3309–3324.

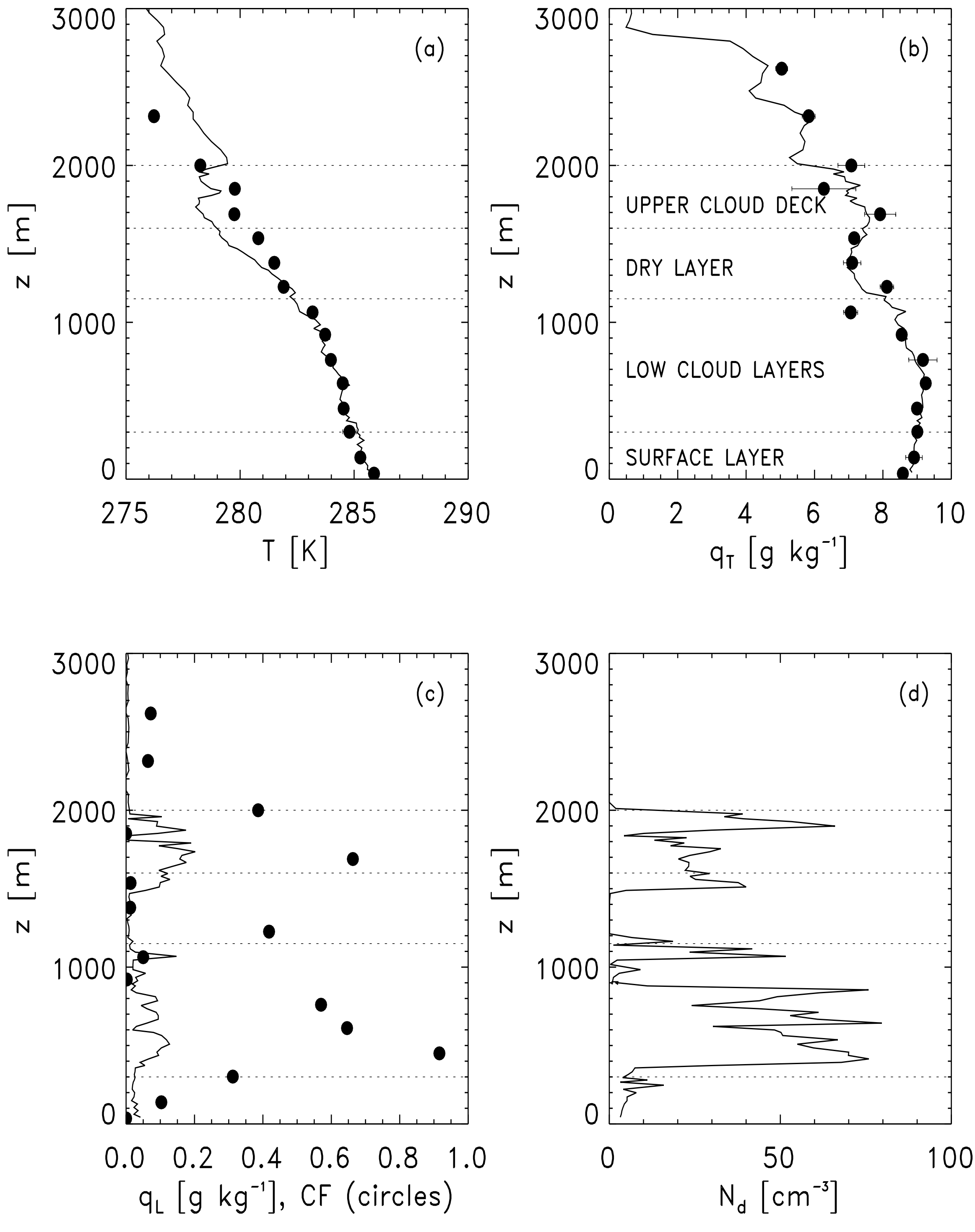

(a)
3000
2000
1000
0
z [m]
275
280
285
290
T [K]
(b)
UPPER CLOUD DECK
DRY LAYER
LOW CLOUD LAYERS
SURFACE LAYER
0
2
4
6
8
10
q_T [g kg^{-1}]
(c)
0.0
0.2
0.4
0.6
0.8
1.0
q_L [g kg^{-1}], CF (circles)
(d)
0
50
100
N_d [cm^{-3}]

Figure 1:

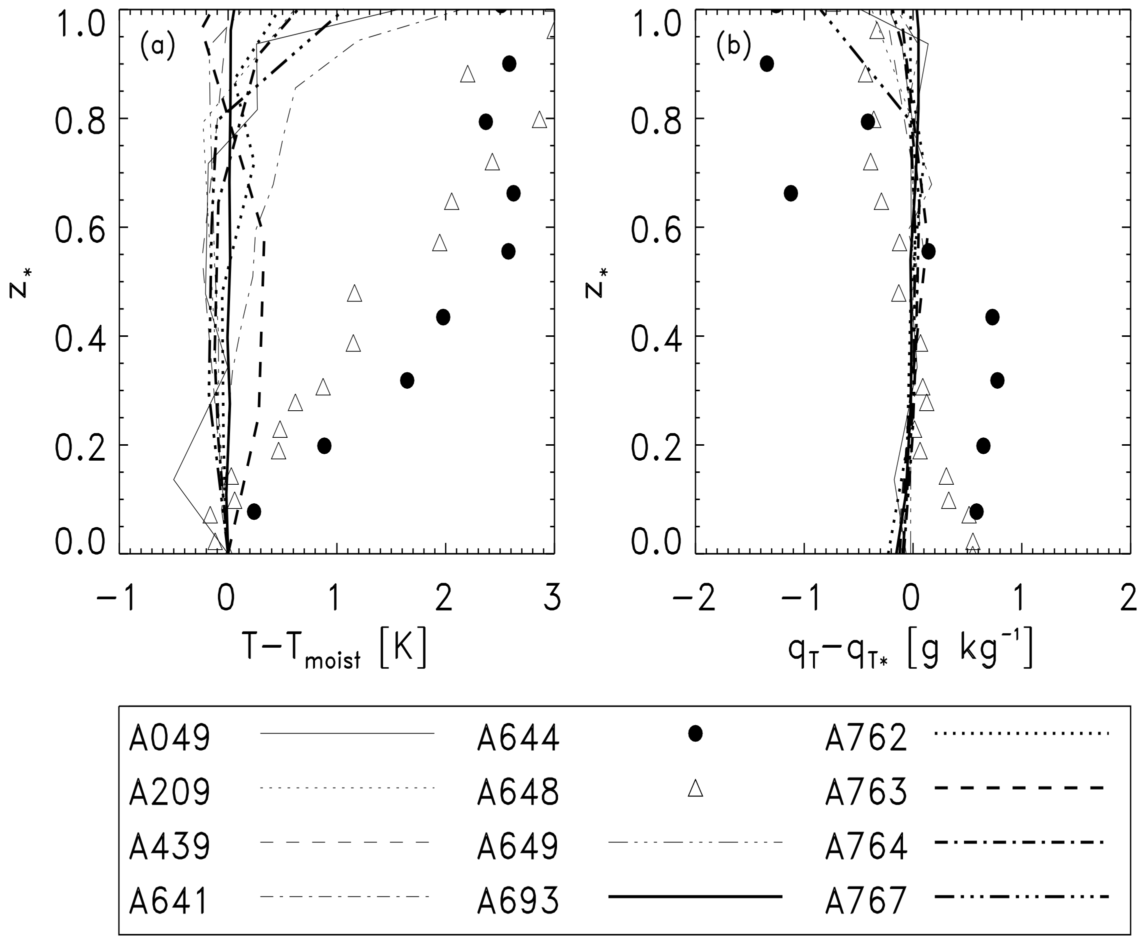

Figure 2: (a) Temperature and (b) total water content in-cloud profiles for each of the cases. Symbols are For (a) the difference between the observed mean temperature at each height and the moist adiabatic temperature is plotted as a function of normalised height. For (b) the difference between the mean total water content at each height and the mean total water content averaged over the entire cloud layer is plotted. The same linestyles and symbols are used throughout this article whenever data from multiple flights are plotted on the same axes.

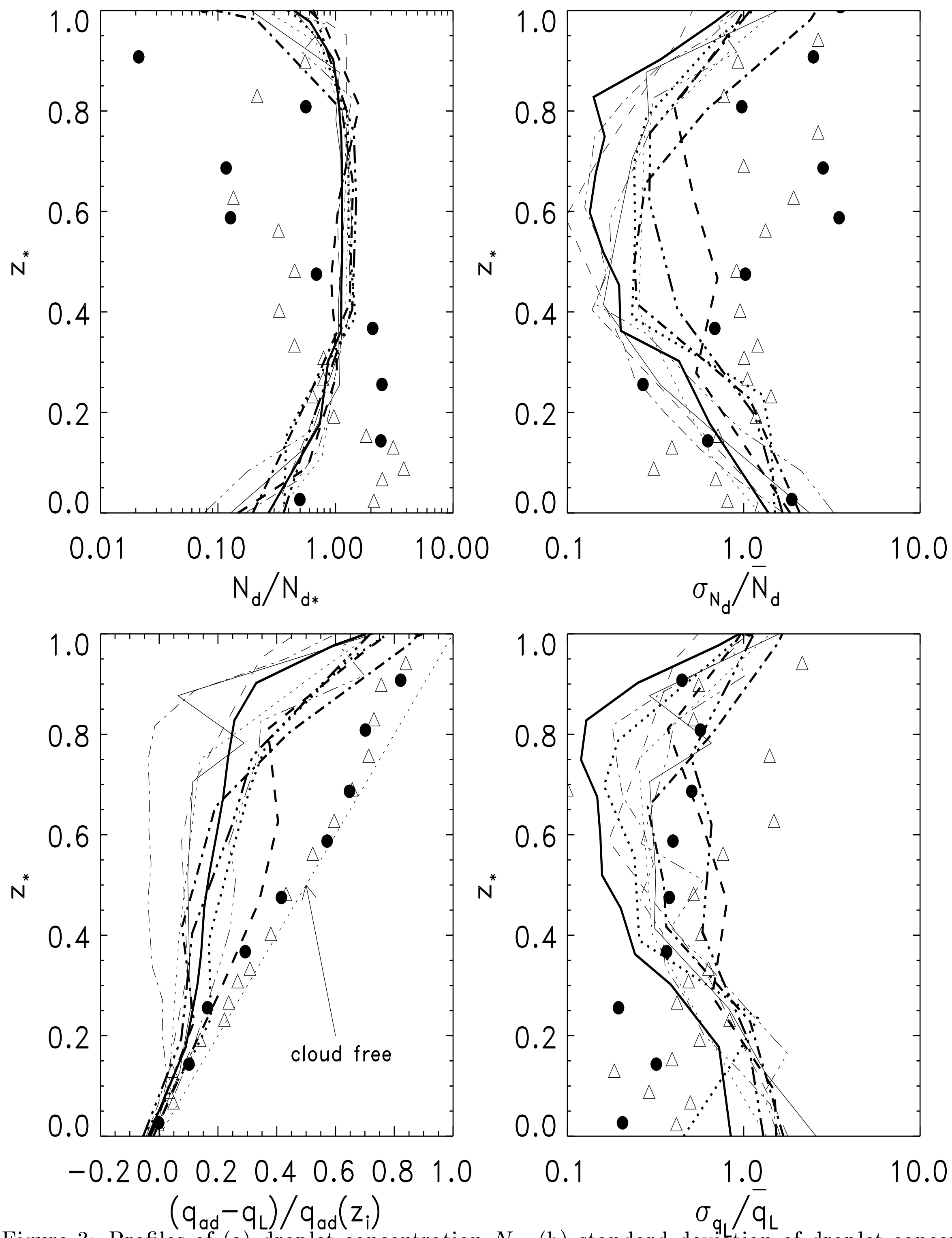

Figure 3: Profiles of (a) droplet concentration N_d, (b) standard deviation of droplet concentration at each level normalised with the mean at each level; (c) values of the subadiabaticity parameter $(q_{ad} - q_L)/q_{ad}(z_i)$ for which zero represents a perfectly adiabatic cloud. The dotted line represents cloud free conditions; (d) the standard deviation of the liquid water content normalised with the mean at that level. Symbolia are the same as for Fig. 2.

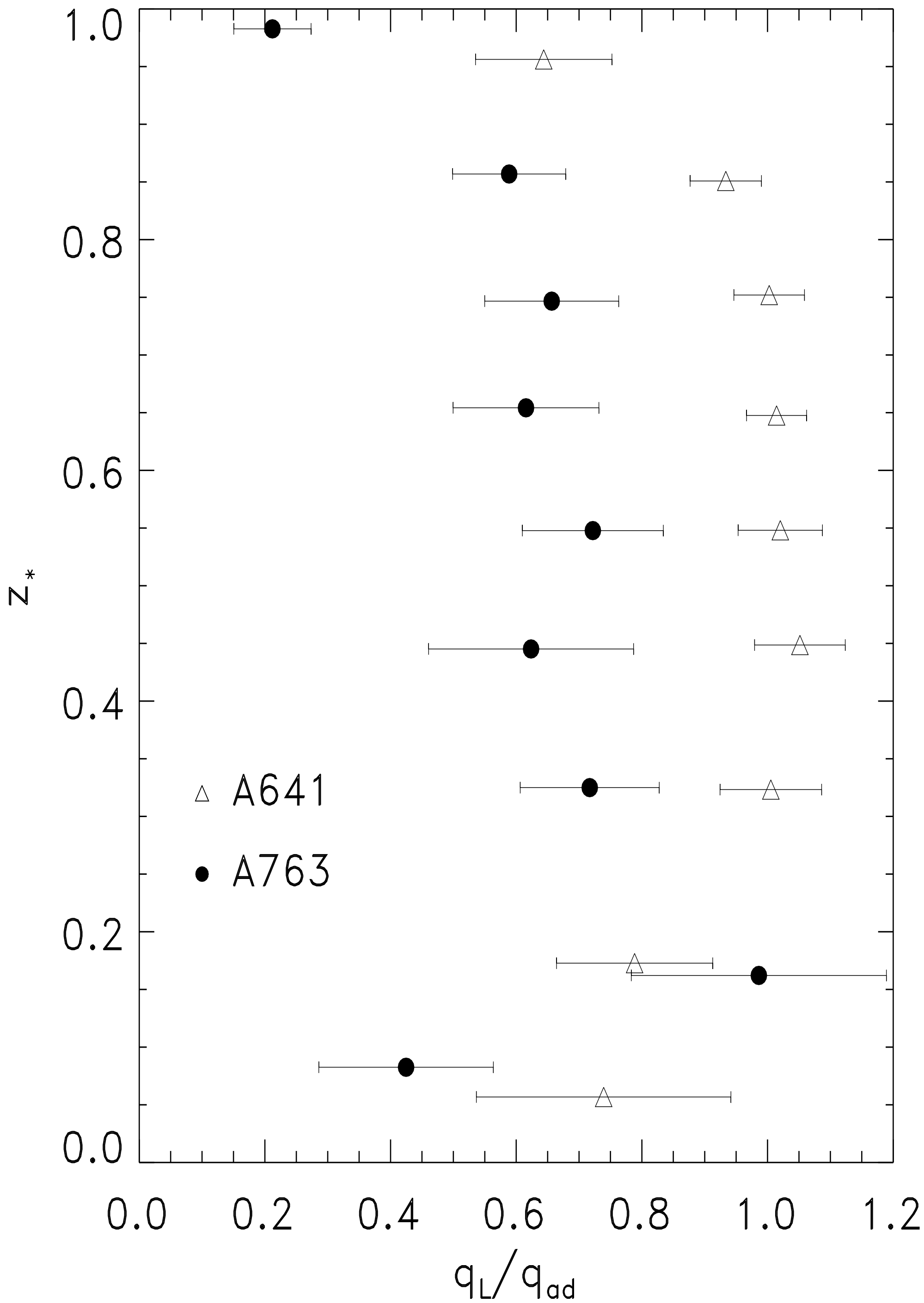

Figure 4: The mean ratio of liquid water content to adiabatic liquid water content (adiabaticity ratio) as a function of height in cases A763 (filled circles) and A641 (triangles), using the individual profile method (see text). These clearly show that the adiabaticity ratio is roughly constant through the bulk of the cloud ($0.2 < z_* < 0.9$). The error bars show the error in the mean (95% confidence level) derived only from the spread in the data values from different profiles. The estimated errors in q_L/q_{ad} derived from a simple model of the cloud structure are ± 0.09 and ± 0.07 (95% level) for A641 and A763 respectively which do not differ markedly from the errors derived from the spread in data.

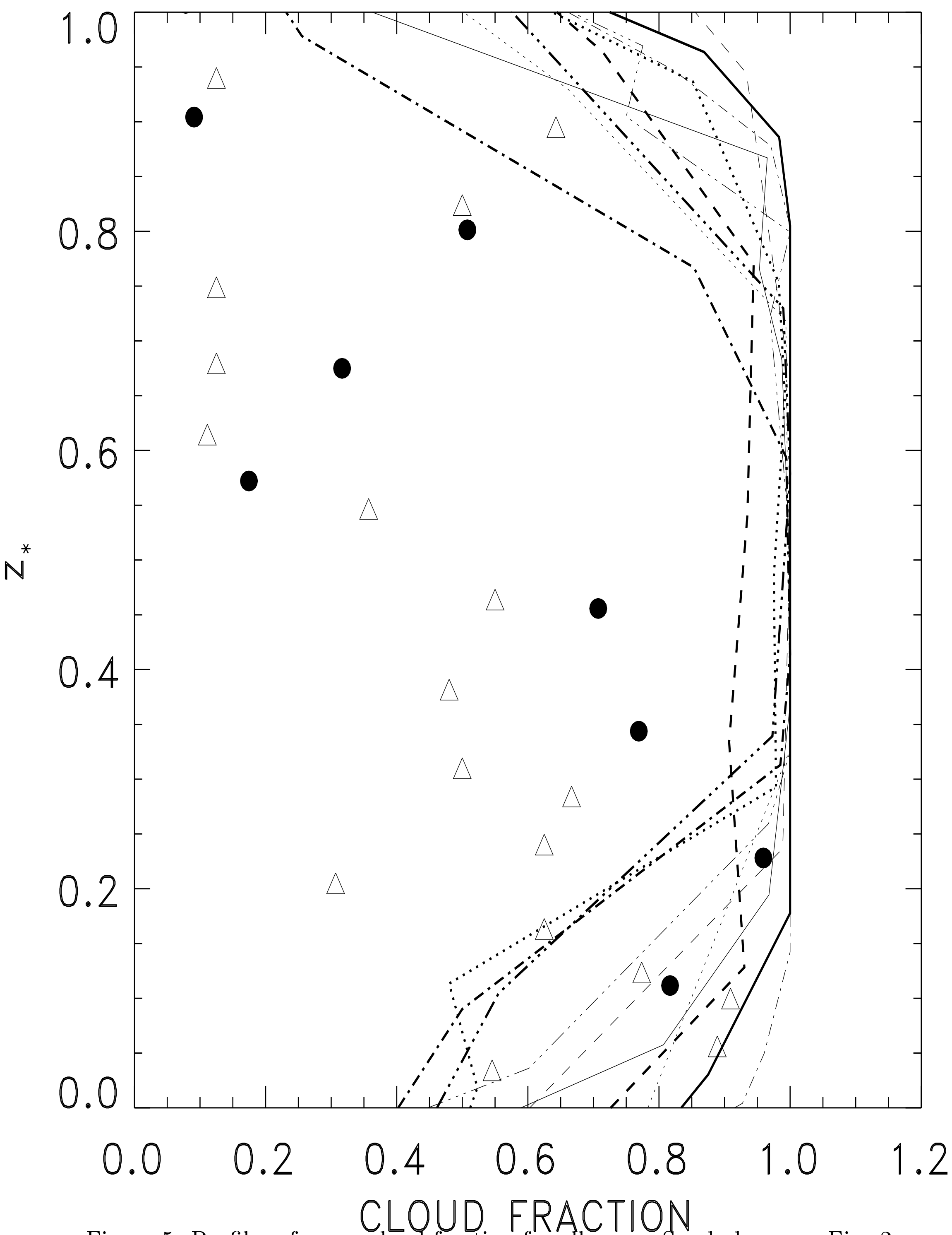

Figure 5: Profiles of mean cloud fraction for all cases. Symbols are as Fig. 2.

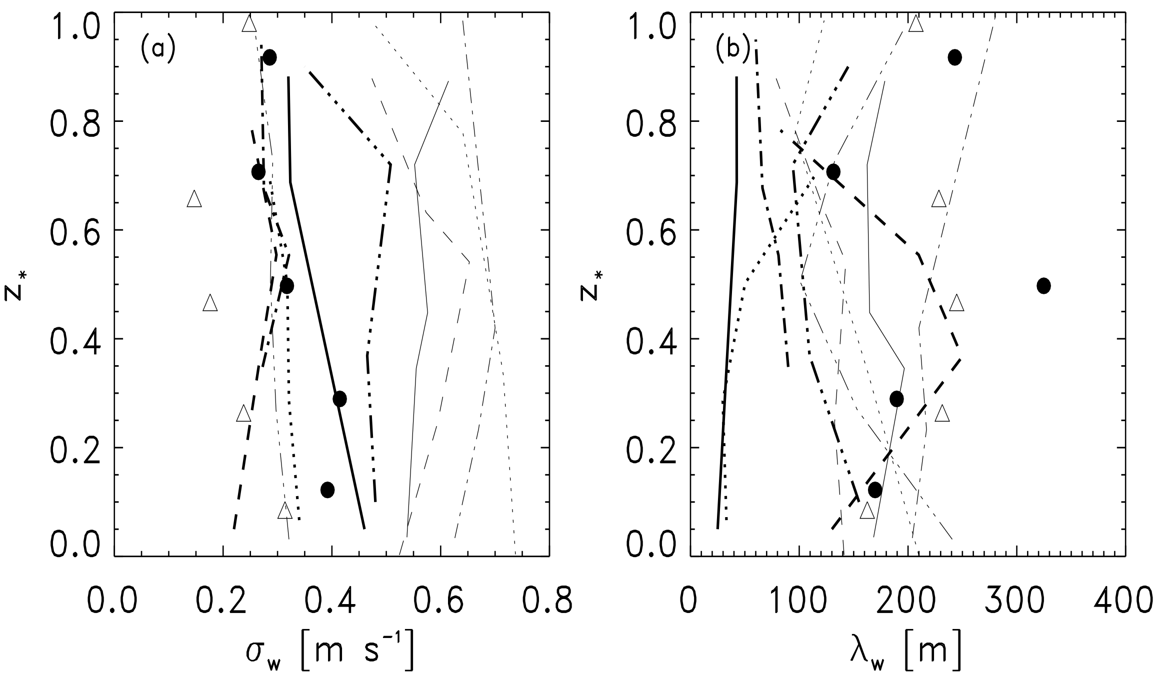

Figure 6: Profiles of vertical wind standard deviation for all cases. Symbols are as Fig. 2.

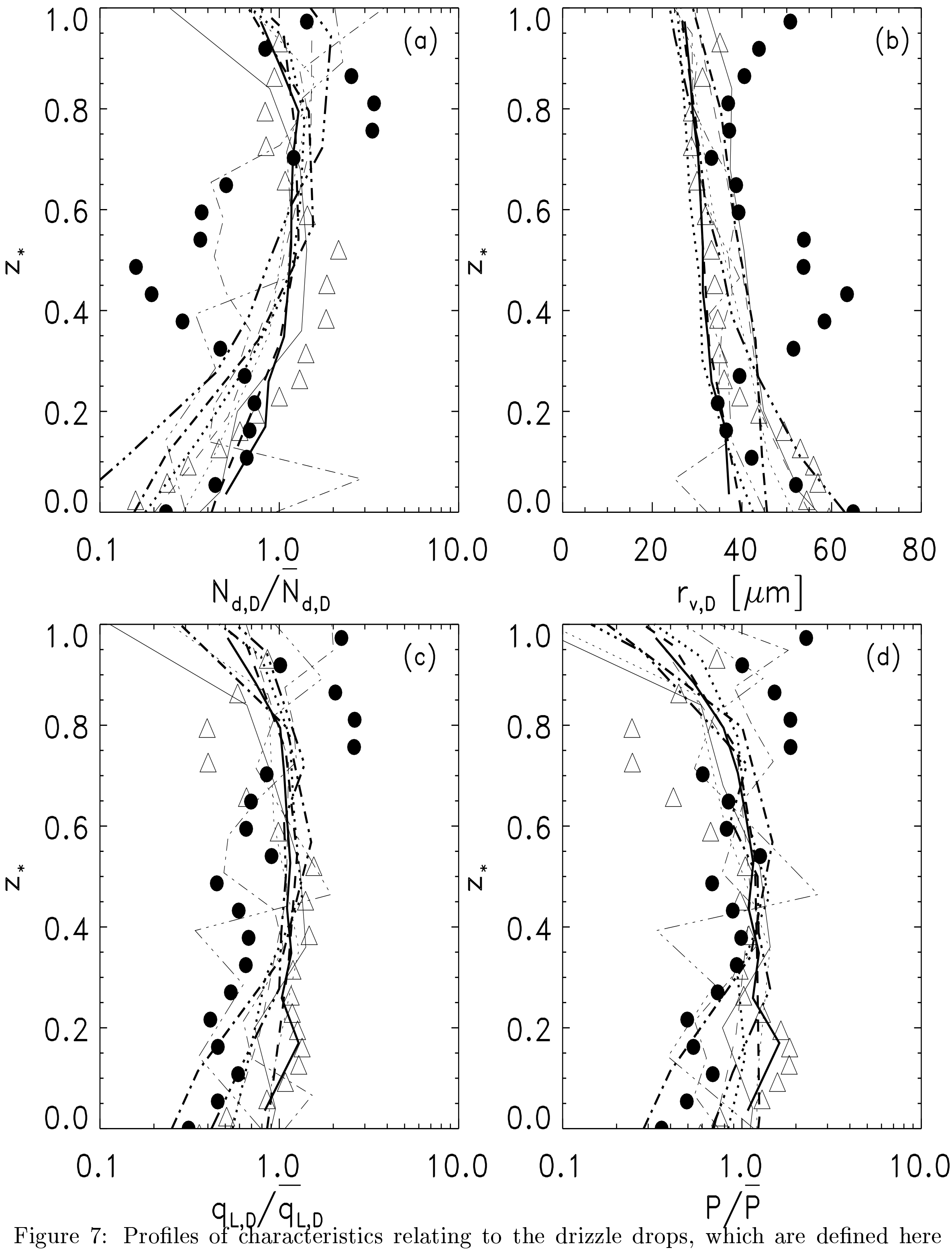

Figure 7: Profiles of characteristics relating to the drizzle drops, which are defined here as drops with radii larger than 20 μm. (a) Drizzle droplet concentration $N_{d,D}$ normalised with the mean drizzle droplet concentration in the cloud layer; (b) volume radius of drizzle drops $r_{v,D}$ which increases towards cloud base; (c) liquid water content contained in the drizzle drops normalised with the mean value for the cloud layer; (d) precipitation rate normalised with the mean value in the cloud layer. Symbols are as Fig. 2.